Available online at www.sciencedirect.com
SCIENCE DIRECT
International Journal of Heat and Mass Transfer 49 (2006) 3408–3416
International Journal of HEAT and MASS TRANSFER
www.elsevier.com/locate/ijhmt

Total concentration approach for three-dimensional diffusion-controlled wet chemical etching

P. Rath [a], J.C. Chai [a,*], H. Zheng [b], Y.C. Lam [a], V.M. Murukeshan [a]

[a] School of Mechanical and Aerospace Engineering, Nanyang Technological University, 50 Nanyang Avenue, 639798, Singapore
[b] Singapore Institute of Manufacturing Technology, 638075, Singapore

Received 25 September 2005; received in revised form 28 February 2006
Available online 11 May 2006

Abstract

A total concentration fixed-grid method is used in this article to model the three-dimensional diffusion-controlled wet chemical etching. A total concentration is defined as the sum of the unreacted and the reacted etchant concentrations. The governing mass diffusion equation based on the total concentration includes the interface condition. The reacted concentration of etchant is a measure of the etchfront position. With this approach the etchfront can be found implicitly. For demonstration purposes, the finite-volume method is used to solve the resulting set of governing equations with initial and boundary conditions. The effect of mask thickness on the etchfront surface evolution is studied. The condition at which a three-dimensional etching is converted into two-dimensional is also presented.

1. Introduction

Etching refers to a process by which material is removed from the substrate itself or any film or layer of material on the substrate surface. Wet chemical etching (WCE) is an etching process that utilizes liquid chemicals which are called etchants, to remove materials from the substrate, usually in specific patterns defined by photoresist mask on the substrate. Materials not covered by the mask are etched away by the chemicals while those covered by the mask are left almost intact. WCE process is generally used in the manufacturing of shadow mask for color-television tubes [1], IC devices in microelectronics industries [2], MEMS devices such as hinges [3] and pressure sensors [4] etc.

Theoretical analysis of the WCE process has important aspects such as the prediction of etchfront (the etchant–substrate interface) which takes a complicated shape in multidimensional etching. Existing mathematical models for WCE process includes the asymptotic solution [5,6], the variational inequality approach [7,8], the moving-grid (MG) approach [7,9,11–14], and the level-set method [15–17]. Recently, a total concentration based fixed-grid method [18–20] is developed to model the WCE. Based on the rate of reaction, two possible cases namely, the diffusion-controlled [5–12,18–20] and the reaction-controlled [7,11–14,19] etching are examined by various researchers. These two cases are studied in the modeling of one-dimensional [9,13,18,19] and two-dimensional [5–12,14,15,17,20] WCE using the above analytical and numerical approaches. The forced and natural convection effects on the etching process are studied by Shin and Economou [11,12].

An asymptotic solution for a two-dimensional WCE is presented by Kuiken [5,6]. The asymptotic solution is valid for diffusion-controlled etching with a large value of the etching parameter, where the interface moves very slowly. Kuiken et al. [9] also presented the exact solution for the diffusion-controlled WCE in a one-dimensional geometry. An analytical treatment based on the perturbation principle is then extended to model a two-dimensional diffusion-controlled WCE. The substrate is partly protected by an infinitely thin semi-infinite mask making it a two-dimensional etching problem. The analytical asymptotic solution is

* Corresponding author. Tel.: +65 6790 4270; fax: +65 6792 4062.
E-mail address: mckchai@ntu.edu.sg (J.C. Chai).

0017-9310/$ - see front matter © 2006 Elsevier Ltd. All rights reserved.
doi:10.1016/j.ijheatmasstransfer.2006.02.053

Nomenclature

a	coefficient of the discretization equation
c	unreacted etchant concentration
C	dimensionless unreacted etchant concentration
c_R	reacted etchant concentration
$c_{R,max}$	maximum possible value of the reacted concentration
c_T	total concentration of etchant
D	diffusion coefficient of etchant
M_{Sub}	molecular weight of the substrate
m	stoichiometric reaction parameter
t	time
t^*	non-dimensional time
$v_{\hat{n}}$	normal speed of the etchant–substrate interface
x, y, z	coordinate directions
X, Y, Z	non-dimensional coordinate directions

Greek symbols

α	under-relaxation factor
β	dimensionless etching parameter
∇	vector differential operator
Δt	time step
ρ_{Sub}	density of the substrate

Subscripts

o	initial
P	control volume P
Sub	the substrate
Et	the etchant
T	total

Superscripts

m	iteration number
o	previous time step

verified with the experiment by etching GaAs in $HCl/H_2O_2/H_2O$ etchant solution [10].

The moving grid (MG) method is a widely used method to model the WCE process. In the MG method, the computational domain is limited to the space occupied by the etchant. Because of the erosion of substrate, it continuously expands with time. The etchant concentration is solved using appropriate boundary conditions and a specified initial condition. Using the interface condition at the etchant–substrate interface, the etchfront velocity is calculated to find the new position of the interface. As the computational domain expands with time, the computation mesh has to be regenerated at every time step. Due to the movement of the mesh, the mesh velocities have to be accounted for in the governing equation in terms of an extra convective term [7,14]. Further, an unstructured mesh system or a body-fitted grid system is needed to model the multidimensional WCE.

The numerical models for two-dimensional WCE are presented by Vuik and Cuvelier [7]. The finite element method (FEM) is used for discretization of the governing equation in the space variables and a finite difference method is used for discretizing the time variable. The MG method and the variational inequality approach are used to track the etchant–substrate interface. The mesh velocities are accounted for in the MG method due to the movements of the computational grids. Bruch et al. [8] parallelize the same etching problem based on the variational inequality approach using a highly efficient parallel algorithm. Shin and Economou [11,12] studied the effect of etchant flow field (forced and natural convection) on the shape evolution of etching cavities. The FEM was used to solve for the etchant velocity distribution and the etchant concentration distribution in the etched cavities. The MG method was used to track the etchant–substrate interface. The extra convective term due to mesh velocities was neglected because of the very slow movement of the interface. Li et al. [13] presented a one-dimensional moving boundary numerical scheme to predict the motion of the etchant–substrate interface while etching phosphosilicate-glass (PSG) with hydrofluoric acid (HF). The model is presented for a radial geometry where a one-dimensional radial diffusion equation is solved using the fully implicit scheme. Kaneko et al. [14] used the MG approach to model a two-dimensional reaction-controlled WCE considering the effect of flowing etchant. A first order reaction kinetic was assumed. The extra convective term due to grid velocities was taken into account in the model. Adalsteinsson and Sethian [15,16] developed a level-set formulation to simulate deposition, etching, and lithography in integrated circuit fabrication using the two-dimensional and three-dimensional models. La Magna et al. [17] used a level-set method for a moving etchfront to simulate two-dimensional profile evolution in WCE process.

Recently, Rath and co-workers [18–20] presented a fixed-grid approach based on the total concentration of the etchant to model the WCE process in one-dimensional (1D) and two-dimensional (2D) geometries. This method is analogous to the enthalpy method used in the modeling of melting/solidification process [21–28]. A total etchant concentration is defined as the sum of the unreacted etchant concentration and the reacted etchant concentration. The governing equation based on the total concentration includes the interface condition. In this formulation, the reacted concentration of etchant is a measure of the etchfront position while etching progresses. The etchfront

can be found implicitly with the total concentration method. Since the grids are fixed, there is no grid velocity. The computational domain includes the whole etchant and substrate domain. Cartesian grid can be used to capture the complicated etchfront evolution in multidimensional etching. The model has been tested for one-dimensional (1D) diffusion-controlled [18] and reaction-controlled [19] WCE and the approach further extends to model two-dimensional (2D) diffusion-controlled etching [20].

In this article, the above total concentration based fixed-grid method is extended to model the three-dimensional (3D) diffusion-controlled WCE. The effect of mask thickness on the etched surface evolution is studied. The condition at which a 3D etchfront is transformed into a 2D etchfront is also examined.

The remainder of this article is divided into six sections. In the next section, a three-dimensional WCE problem, the governing equation, the interface condition and the boundary conditions are described. Various ingredients of the proposed fixed-grid method are then discussed. A brief description of the numerical method used in this article is given. The overall solution procedure is then summarized. Discussion of the results obtained using the proposed fixed-grid method is presented. Some concluding remarks are then given.

2. Problem description and governing equations

The schematic and computational domain for the three-dimensional etching problem considered is shown in Fig. 1. An opening of square cross section ($2a \times 2a$) is to be etched in a substrate (Fig. 1a). The remainder of the substrate surface is covered by a photoresist mask at the top. For demonstration purposes, the width of the masks on all the four sides of the opening is located sufficiently far from the opening so that the concentration of etchant far away from the opening will remain unaltered at the initial etchant concentration. The initial concentration of the etchant at $t = 0$ is c_o. The etchant solution is assumed to be stationary, i.e., the convection effect is neglected. At $t > 0$, the reaction between the etchant and the substrate at the etchant–substrate interface results in the reduction of the concentration

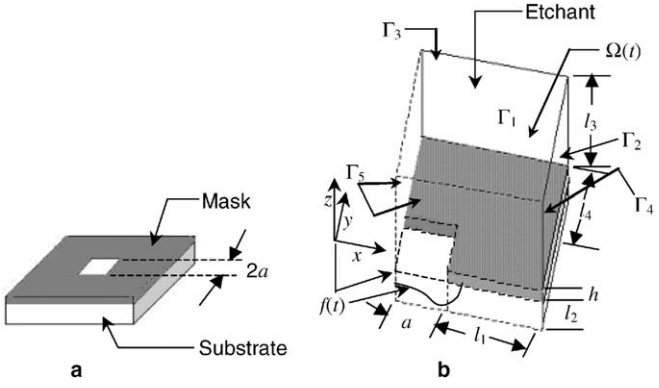

Fig. 1. Schematic and computational domain of the three-dimensional (3D) etching: (a) schematic; (b) the computational domain.

of etchant adjacent to the etchant–substrate interface and the depletion of the substrate. The concentration of etchant on the boundaries far away from the opening is kept at the initial concentration, i.e., $c = c_o$. The etching is assumed diffusion-controlled, which is associated with infinitely fast reaction rate at the interface. The origin of the coordinate system is set to the etchant–substrate interface at the center of the opening. Since the problem is symmetrical about the origin, only one-quarter of the domain is considered, as shown in Fig. 1b. The governing equation, the interface condition and the boundary conditions are presented next.

2.1. Governing equation

For a stationary etchant solution, the etchant concentration within the etchant domain is governed by the mass diffusion equation given by

$$\frac{\partial c}{\partial t} = \frac{\partial}{\partial x}\left(D\frac{\partial c}{\partial x}\right) + \frac{\partial}{\partial y}\left(D\frac{\partial c}{\partial y}\right) + \frac{\partial}{\partial z}\left(D\frac{\partial c}{\partial z}\right) \quad \text{in } \Omega(t) \tag{1a}$$

The initial and boundary conditions are

Initial condition at $t = 0$

$$c = c_o \quad \text{in } \Omega(0) \tag{1b}$$

Boundary conditions for $t > 0$

$$c = c_o \quad \text{on } \Gamma_1, \Gamma_2 \text{ and } \Gamma_3 \tag{1c}$$

$$\frac{\partial c}{\partial n} = 0 \quad \text{on } \Gamma_4(t) \text{ and } \Gamma_5(t) \tag{1d}$$

$$c = 0 \quad \text{on f(t)} \tag{1e}$$

Interface condition for $t > 0$ *on* $f(t)$

The interface condition is obtained by the balance between rate of diffusion and rate of reaction at the etchant–substrate interface. Neglecting the effect of the change in energy due to the etching of the front, gives the interface velocity as

$$\vec{v} = -\frac{DM_{\text{Sub}}}{m\rho_{\text{Sub}}}\nabla c \tag{1f}$$

where $\vec{v}$ is the velocity of the etchant–substrate interface, D is the diffusion coefficient of etchant, M_{Sub} is the molecular weight of the substrate, ρ_{Sub} is the density of the substrate and m is the stoichiometric reaction parameter of the etchant–substrate reaction. The normal speed of the etchant–substrate interface $v_{\hat{n}}$ is obtained by dotting both sides of Eq. (1f) with the unit vector $\hat{n}$ normal to the interface which points towards the substrate region. This can be written as

$$\vec{v}\cdot\hat{n} = -\frac{DM_{\text{Sub}}}{m\rho_{\text{Sub}}}\nabla c\cdot\hat{n} \Rightarrow v_{\hat{n}} = -\frac{DM_{\text{Sub}}}{m\rho_{\text{Sub}}}\frac{\partial c}{\partial \hat{n}} \tag{1g}$$

3. The total concentration method

In the proposed approach, the *total concentration* includes the reacted and the unreacted etchant concentration. This is defined as

$$c_T \equiv c + c_R \tag{2}$$

where c_T is the total concentration, c is the unreacted etchant concentration and c_R is the reacted etchant concentration, respectively. Physically, c_R is the etchant concentration *consumed* in the reaction process. As such it is constant except at the etchant–substrate interface. This is used to capture the etchfront implicitly. The value of c_R changes from 0 to its maximum possible value of $c_{R,max}$ in a control volume where etching is taking place. The maximum possible value of the reacted concentration termed $c_{R,max}$, is the amount of etchant required per unit volume of substrate to dissolve the substrate during reaction. In a unit volume, there are ρ_{Sub}/M_{Sub} moles of substrate. The reaction between the etchant and the substrate is given as

$$S + mE \rightarrow qP \tag{3}$$

where S is the substrate, E is the etchant and P is the product, respectively. From Eq. (3) it is seen that the amount of etchant needed to dissolve a unit volume of substrate is $m\rho_{Sub}/M_{Sub}$. As $c_{R,max}$ is the amount of etchant required per unit volume of substrate to dissolve the substrate during reaction, it can be written as

$$c_{R,max} = \frac{m\rho_{Sub}}{M_{Sub}} \tag{4}$$

The governing equation based on the total concentration can be written as

$$\frac{\partial c_T}{\partial t} = \frac{\partial}{\partial x}\left(D\frac{\partial c}{\partial x}\right) + \frac{\partial}{\partial y}\left(D\frac{\partial c}{\partial y}\right) + \frac{\partial}{\partial z}\left(D\frac{\partial c}{\partial z}\right) \tag{5}$$

Using Eq. (2), Eq. (5) can be rearranged as

$$\frac{\partial c}{\partial t} = \frac{\partial}{\partial x}\left(D\frac{\partial c}{\partial x}\right) + \frac{\partial}{\partial y}\left(D\frac{\partial c}{\partial y}\right) + \frac{\partial}{\partial z}\left(D\frac{\partial c}{\partial z}\right) - \frac{\partial c_R}{\partial t} \tag{6}$$

This equation is valid in both the etchant and the substrate regions. The interface condition given by Eq. (1g) is contained in Eq. (6) implicitly. The detailed derivation of the interface condition from the governing equation is described in the previous article [19].

3.1. Procedure to update c_R

A procedure to evaluate the reacted etchant concentration c_R is presented in this section. The reacted concentration is constant away from the etchant–substrate interface. Hence, Eq. (6) reduces to the original governing equation (Eq. (1a)) except at the etchant–substrate interface. At the etchant–substrate interface, the reacted etchant concentration is a measure of the amount of substrate being etched. In the proposed FG method, the control volumes where etching is taking place are identified and are called as the etching-control-volume (ECV). The ECVs are the substrate control volumes adjacent to the etchant control volumes. In an ECV, c_R changes from 0 to its maximum possible value of $c_{R,max}$. An iterative procedure to update c_R in an ECV is described in this section. The finite-volume discretization equation (using the fully implicit scheme) of Eq. (6) for an ECV (the control volume P) is given as

$$a_P c_P^m = \sum a_{nb} c_{nb}^m + a_P^o c_P^o - (c_{R,P}^m - c_{R,P}^o)\frac{\Delta V_P}{\Delta t} \tag{7}$$

where m is the mth iteration of the current time step, o is the previous time step, P is the control volume P, nb is the neighboring control volumes, a is the coefficients of the discretization equation, ΔV is the volume of a control volume and Δt is the time step. Eq. (7) is valid for all control volumes. However, as c_R is constant in the etchant and substrate domains, the last term on the right side of Eq. (7) is zero except in the ECVs. At the $(m+1)$th iteration, Eq. (7) can be written as

$$a_P c_P^{m+1} = \sum a_{nb} c_{nb}^{m+1} + a_P^o c_P^o - (c_{R,P}^{m+1} - c_{R,P}^o)\frac{\Delta V_P}{\Delta t} \tag{8}$$

Subtracting Eq. (8) from Eq. (7) and rearranging, gives

$$c_{R,P}^{m+1} = c_{R,P}^m + \frac{\Delta t}{\Delta V_P}\left[a_P(c_P^m - c_P^{m+1}) + \sum a_{nb}(c_{nb}^{m+1} - c_{nb}^m)\right] \tag{9}$$

When the solution converges, the last term of Eq. (9) will be zero. However, during the initial iteration process, it is most likely a non-zero term. Realizing that it is zero upon convergence, this term can be ignored from the calculation and Eq. (9) becomes

$$c_{R,P}^{m+1} = c_{R,P}^m + \alpha a_P \frac{\Delta t}{\Delta V_P}(c_P^m - c_P^{m+1}) \tag{10}$$

where α is an under-relaxation factor whose value lies between 0 and 1. For a diffusion-controlled reaction, the reaction rate at the interface is infinitely fast which makes the concentration at the interface to become zero. For diffusion-controlled reaction, the current procedure ensures that $c_P^{m+1} = 0$ and the excess concentration is used to update the reacted concentration. With $c_P^{m+1} = 0$, Eq. (10) becomes

$$c_{R,P}^{m+1} = c_{R,P}^m + \alpha a_P \frac{\Delta t}{\Delta V_P} c_P^m \tag{11}$$

Within the control volume where etching is taking place, the reacted concentration is updated using Eq. (11). The etching for a given ECV completed, when $c_{R,P}^{m+1}$ reaches $c_{R,max}$.

4. Numerical method

In this article, the finite-volume method (FVM) of Patankar [29] is used to solve the governing mass diffusion equation. Since a detailed discussion of the FVM is available in Patankar [29], only a brief description of the major features of the FVM used is given here. In the FVM, the domain is divided into a number of control volumes such that there is one control volume surrounding each grid point. The grid point is located in the center of a control volume. The governing equation is integrated over each control volume to

derive an algebraic equation containing the grid point values of the dependent variable. The discretization equation then expresses the conservation principle for a finite control volume just as the partial differential equation expresses it for an infinitesimal control volume. The resulting solution implies that the integral conservation of mass is exactly satisfied for any control volume and of course, for the whole domain. The resulting algebraic equations are solved using a line-by-line Tri-diagonal Matrix Algorithm. In the present study, a solution is deemed converged when the maximum change in the concentration and the maximum change in the reacted concentration between two successive iterations are less than 10^{-11}.

5. Overall solution procedure

The overall solution procedure for the proposed total concentration method can be summarized as follows:

1. Specify the etchant domain, the substrate domain and the mask region. Ensure that the etchant–substrate interface lies on the interface between two control volumes.
2. Set the initial etchant concentration as c_o in the etchant domain and zero in the substrate domain including the mask region.
3. Initially set c_R to 0 in the substrate domain including the mask region and to $c_{R,max}$ in the etchant domain, respectively.
4. Advance the time step to $t + \Delta t$.
5. Identify the etching control volumes (ECVs). These are the substrate control volumes with adjacent etchant control volumes.
6. Set the unreacted etchant concentration to zero in the mask and substrate regions (except the ECVs). One possible way to do this is by adding a big number in the denominator term while evaluating the concentration at a given node point using the "internal" boundary condition approach of Patankar [29].
7. Solve Eq. (6) for the unreacted etchant concentration.
8. Update the reacted concentration in the ECVs using Eq. (11).
9. Check for convergence.
   (a) If the solution has converged, then check if the required number of time steps has been reached. If yes, stop. If not, repeat Eqs. (4)–(9).
   (b) If the solution has not converged, then check the calculated reacted concentration.
   - If $c_R < c_{R,max}$, repeat Eqs. (7)–(9).
   - If $c_R \geqslant c_{R,max}$, then set $c_R = c_{R,max}$ and repeat Eqs. (5)–(9).

6. Results and discussion

Fig. 1 shows the schematic of the 3D-etching problem, which is solved using the proposed total concentration method. Due to the symmetry of the problem about the origin, only one-quarter of the domain is modeled as shown in Fig. 1b. The dimensionless variables used for presentation of results are defined below.

$$X \equiv x/a \tag{12a}$$

$$Y \equiv y/a \tag{12b}$$

$$Z \equiv z/a \tag{12c}$$

$$C \equiv c/c_o \tag{12d}$$

$$t^* \equiv tD/a^2 \tag{12e}$$

$$\beta \equiv m\rho_{Sub}/c_o M_{Sub} \tag{12f}$$

In Eq. (12f), β is the dimensionless etching parameter. It is a measure of the initial etchant concentration for a given substrate to be etched. As seen from Eq. (12f), the initial etchant concentration (c_o) is inversely proportional to β. The speed of the etchfront is also inversely proportional to β. This relation can be obtained from the interface condition (Eq. (1g)) using the above dimensionless variables. So, a high initial etchant concentration leads to lower value of β, which in turn increases the speed of the etchfront. A

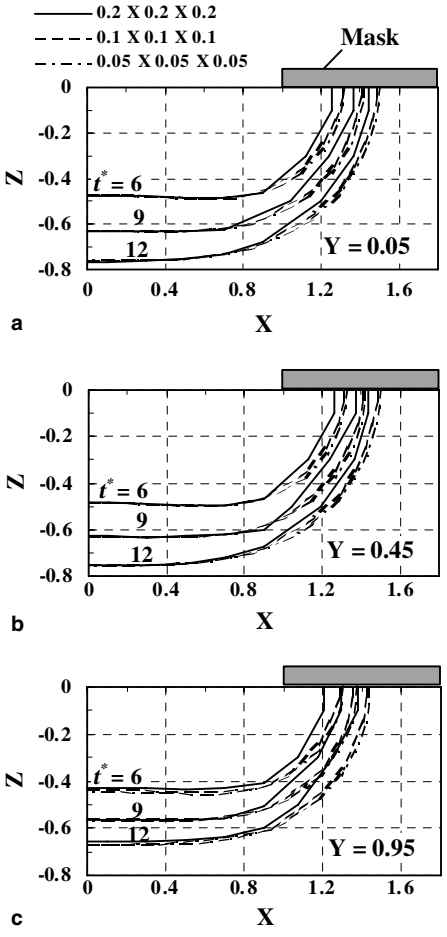

Fig. 2. Grid independent study at three different locations in YZ-plane for $\beta = 10$: (a) section of the etchfront at $Y = 0.05$ from the origin; (b) section of the etchfront at $Y = 0.45$ from the origin; (c) section of the etchfront at $Y = 0.95$ from the origin.

substrate having dimensionless cross-section $\{1 + L_1(l_1/a)\} \times \{1 + L_4(l_4/a)\}$ and dimensionless height $L_2(l_2/a)$ is to be etched with an opening cross-section 1×1, which is exposed to etchant as shown in Fig. 1b. The remainder of the substrate is covered with a photoresist mask at the top to protect it from direct contact with the etchant. The dimensionless lengths L_1 and L_4 are taken 6.5 each. The dimensionless thickness of the substrate, L_2 is taken as 2. The dimensionless height of etchant is taken as $L_3 = l_3/a = 6.5$. Two mask thicknesses namely, infinitely thin and finite mask thicknesses are chosen for presentation of the results. For infinitely thin mask, the non-dimensional mask thickness is taken as $H = h/a = 0.005$. Although not shown, a further decrease in mask thickness does not alter the solution. For finite mask thickness, the thickness of the mask is taken as one-fifth of the substrate thickness, i.e., $H = h/a = 0.4$.

A grid refinement study is performed to ensure the solutions are grid independent: temporal as well as spatial. Fig. 2 shows the evolution of the sectional etchfronts at three different sections at distances 0.05, 0.45 and 0.95 from the origin in *XZ*- and *YZ*-plane cuts at three time levels. The dimensionless etching parameter β (defined in Eq. (12f)) is 10 and the mask is infinitely thin. Three control volume sizes namely, $0.2 \times 0.2 \times 0.2$, $0.1 \times 0.1 \times 0.1$ and $0.05 \times 0.05 \times 0.05$ are taken to perform this test. These control volume sizes are taken near the opening region of the substrate. An expanding grid is used away from the opening, as the grid sizes away from the etchant–substrate interface have no significant effect on the solution. For each control volume size the time independent etchfronts are shown. The time step size for all three control volume sizes is found to be $\Delta t^* = 0.01$. It is seen that there is no significant difference in the prediction of etchfront from control volume sizes of $0.1 \times 0.1 \times 0.1$ and $0.05 \times 0.05 \times 0.05$. As a result, $0.1 \times 0.1 \times 0.1$ control volume sizes are used in this article. Since the quantitative results for three-dimensional etching are not available in the literature, hence the comparison of the etchfront predictions is shown for a two-dimensional case as discussed in the last paragraph of this section.

Fig. 3 shows the sections of the etchfronts taken from two perpendicular planes namely, *XZ* and *YZ*. Etchfronts are shown at three different sections at distances 0.05, 0.45 and 0.95 from the origin. It is seen that the sections of the etchfronts taken from the above two perpendicular planes at equal distances from the origin are same. This is in accordance with the symmetry of the problem considered

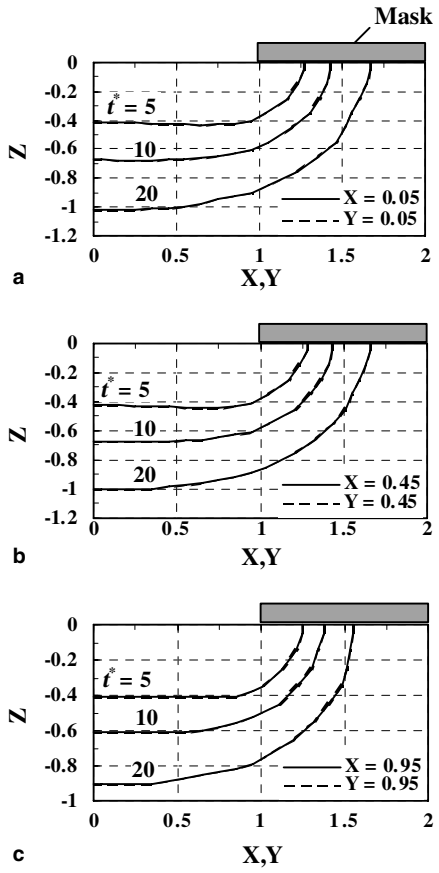

Fig. 3. Etchfronts at three different sections in *XZ*- and *YZ*-plane cuts for $\beta = 10$: (a) sections of etchfronts at distances of 0.05 from the origin; (b) sections of etchfronts at distances of 0.45 from the origin; (c) sections of etchfronts at distances of 0.95 from the origin.

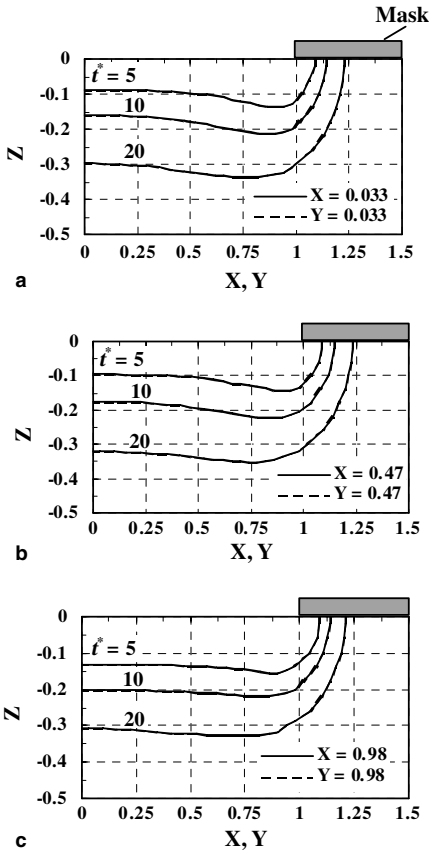

Fig. 4. Etchfronts at three different sections in *XZ*- and *YZ*-plane cuts for $\beta = 50$: (a) sections of etchfronts at distances of 0.033 from the origin; (b) sections of etchfronts at distances of 0.47 from the origin; (c) sections of etchfronts at distances of 0.98 from the origin.

here. Since the boundary conditions in two perpendicular planes are symmetrical and the opening is also square (1×1) in size, hence the etchfronts are also symmetrical in two perpendicular planes (XZ and YZ) at equal distances from the origin. The bulging effect is pronounced near the mask corner at an early time ($t^* = 5$) as shown in Fig. 3. This is because of the faster diffusion rate of etchant near the mask corner. As time increases, the bulging region expands towards the origin. Fig. 4 shows the sections of etchfronts for $\beta = 50$. The etch depth in this case is relatively small compared to the former case. This is because of the decrease in the initial etchant concentration (c_o) with increase in β value for a given etchant–substrate combination. This is evident from Eq. (12f), as β is inversely proportional to the initial etchant concentration. When the value of β increases to 50, the bulging effect is more clearly seen even for longer time compared to $\beta = 10$. This is because of the narrowing of the bulging region with increase in the value of β.

Figs. 5 and 6 show the evolution of etch surfaces with time for infinitely thin and thick mask conditions, respectively. The etching parameter β is 50. It is seen that the bulging of etched surfaces is not pronounced when mask thickness is finite. The vertical etch depth is nearly uniform along the etched surfaces. This is because of the large diffusion length of etchant particles near the mask corner due to finite mask thickness. Therefore, the effect of the diffusion of etchant to the interface from the sides of the mask is less compared to the diffusion of etchant to the interface from top. Hence fresh etchant is less readily available near the mask corner as thickness of the mask increases which results in a slow etch rate near the mask corner. As a result, the etchfront moves at a nearly constant speed in the vertical direction (Z-direction). Therefore, the bulging is not pronounced even at early times unlike the case with infinitely thin mask where bulging is pronounced near the mask corner at early etching time.

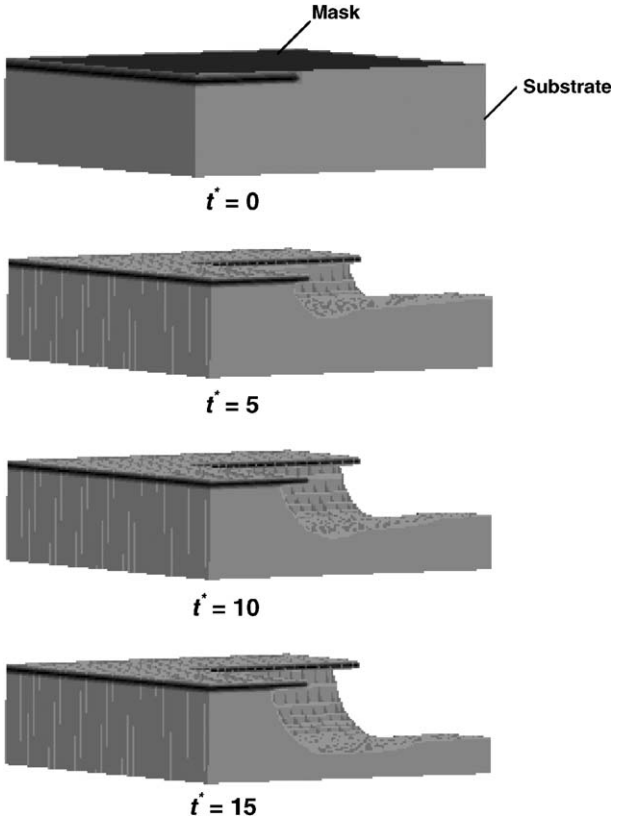

Fig. 5. Evolution of etched surface at different times during etching with infinitely thin mask ($H = 0.005$) and $\beta = 50$.

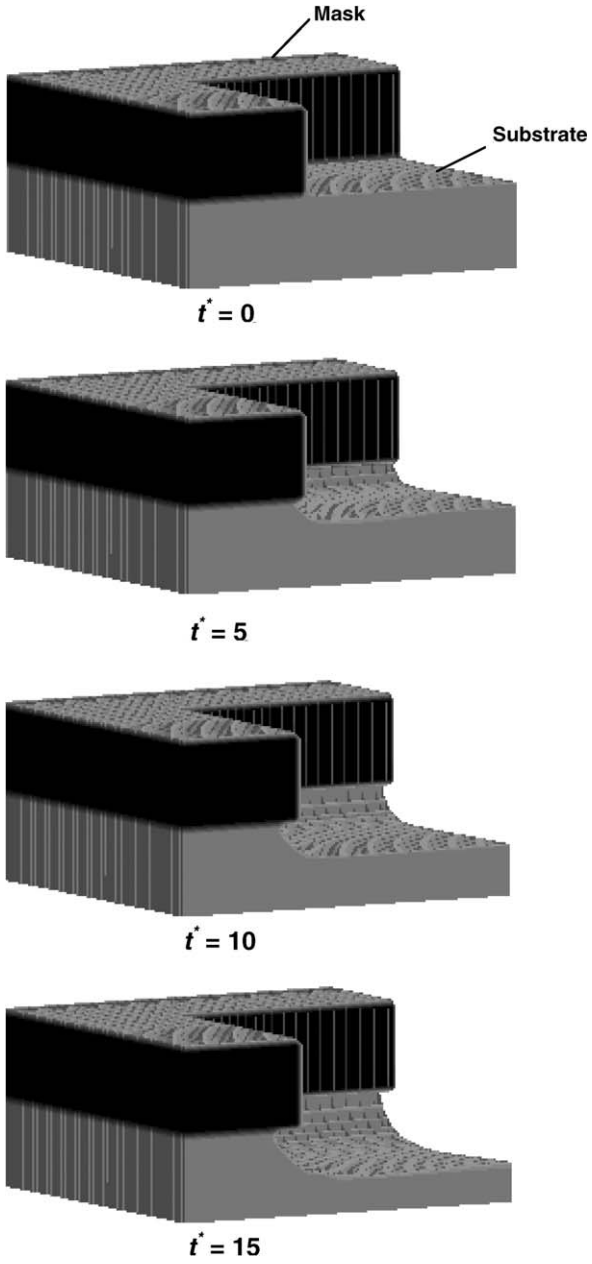

Fig. 6. Evolution of etched surface at different times during etching with finite mask thickness ($H = 0.4$) and $\beta = 50$.

Fig. 7 shows the concentration distribution at $t^* = 20$ for $\beta = 10$ and infinitely thin mask. The etchant–substrate interface is near the contour $C = 0.05$. The etchant

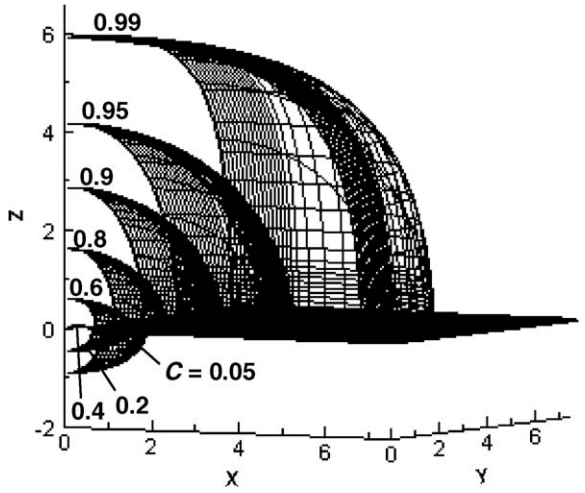

Fig. 7. Concentration contours at $t^* = 20$ for $\beta = 10$ and infinitely thin mask.

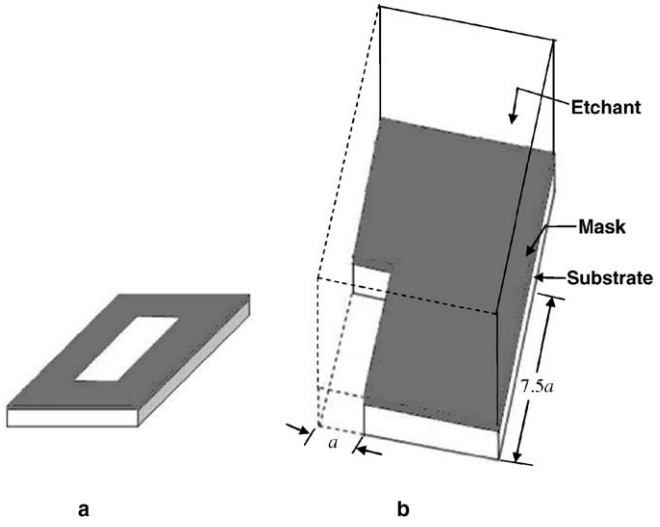

Fig. 8. Schematic for conversion of 3D-etching problem to a 2D-etching problem: (a) schematic; (b) the computational domain.

concentration is less near the etchant–substrate interface compared to away from the interface and is nearly unchanged with initial etchant concentration far away from the interface. This is because of the consumption of etchant at the interface to dissolve the substrate during etchant–substrate reaction.

The schematic of the problem considered to study the transformation of a 3D-etching problem to a 2D-etching problem is shown in Fig. 8. A substrate covered with a photoresist mask at the top leaving behind a rectangular opening (Fig. 8a), which is exposed for direct contact of etchant with the substrate. The cross-sectional dimension of the opening is taken as $2a \times 15a$. Because of the symmetry of the problem about the center of the opening, only one-quarter of the domain is considered with the origin set at the center as shown in Fig. 8b. The boundary conditions are same as discussed in the schematic of the previous problem. Fig. 9 shows the evolution of the etched surface at $t^* = 20$ for $\beta = 10$. It is seen that away from the mask corner (towards the origin) in the y-direction, the vertical etch depth is almost constant. The effect of the diffusion of etchant at the mask corner (due to the consumption of etchant at the interface) does not significantly affect the etchant concentration far away from the mask corner in the y-direction. Hence the etch depth is nearly uniform far away from the mask corner towards the origin. Fig. 10 shows the cross-section of the etchfronts at different time levels taken from the YZ-plane near the origin. Fig. 10a shows the comparison of the sectional etchfronts near the origin with the 2D-etchfronts obtained using the total concentration based FG method [20] and Fig. 10b shows the comparison with the 2D-etchfronts

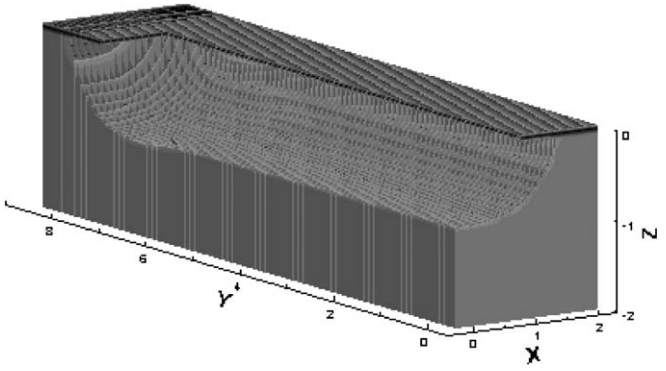

Fig. 9. Evolution of an etched surface in a rectangular opening at $t^* = 20$ for $\beta = 10$.

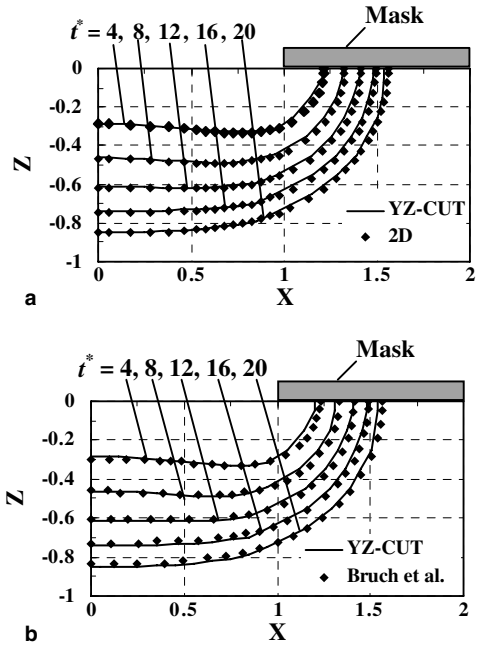

Fig. 10. Comparison of the sections of 3D-etchfronts (taken from YZ-plane near the origin) with the 2D-etchfronts for $\beta = 10$: (a) comparison with 2D etchfronts obtained using the FG method [20]; (b) Comparison of sectional etchfronts with 2D etchfronts of Bruch et al. [8].

of Bruch et al. [8]. It is seen that the sections of the etchfronts from *YZ*-plane near the origin are actually giving the 2D-etchfronts. Hence it can be said that, the 3D-etchfronts transformed to 2D-etchfronts away from the mask corner.

7. Concluding remarks

A fixed-grid method based on the total concentration of etchant (called the total concentration method) has been used to model the three-dimensional WCE. The proposed method is analogous to the enthalpy method used in the modeling of melting/solidification processes. Some key ingredients of the proposed total concentration method are discussed. The governing mass diffusion equation based on the total concentration includes the interface condition. With this proposed method the etchfront position can be found implicitly. The method has been applied to three-dimensional diffusion-controlled etching. The finite-volume method is used to discretize the governing equation. The results obtained from the proposed approach are discussed and a possible situation for the transformation of a three-dimensional etching problem to two-dimensional etching problem is also presented.

References

[1] K.H. Hoffman, J. Sprekels, Free boundary problems: theory and applications, Longman Sci. Tech. 1 (1990) 89.
[2] M.J. Madou, Fundamentals of Microfabrication, second ed., CRC Press, New York, 2002.
[3] K.S.J. Pister, M.W. Judy, S.R. Burgett, R.S. Fearing, Microfabricated hinges, Sens. Actuat. A 33 (1992) 249–256.
[4] C.H. Mastrangelo, X. Zhang, W.C. Tang, Surface micromachined capacitive differential pressure sensor with lithographically-defined silicon diaphragm, The Eighth International Conference on Solid-State Sensors and Actuators, Eurosensor IX, Stockholm, June 25–29, 1995, pp. 612–615.
[5] H.K. Kuiken, Etching: a two-dimensional mathematical approach, Proc. R. Soc. Lond. A 392 (1984) 199–225.
[6] H.K. Kuiken, Etching through a slit, Proc. R. Soc. Lond. A 396 (1984) 95–117.
[7] C. Vuik, C. Cuvelier, Numerical solution of an etching problem, J. Comput. Phys. 59 (1985) 247–263.
[8] J.C. Bruch Jr., C.A. Papadopoulos, J.M. Sloss, Parallel computing used in solving wet chemical etching semiconductor fabrication problems, GAKUTO International Series, Math. Sci. Appl. 1 (1993) 281–292.
[9] H.K. Kuiken, J.J. Kelly, P.H.L. Notten, Etching profiles at resist edges – I. Mathematical models for diffusion-controlled cases, J. Electrochem. Soc. 133 (1986) 1217–1226.
[10] P.H.L. Notten, J.J. Kelly, H.K. Kuiken, Etching profiles at resist edges – II. Experimental confirmation of models using GaAs, J. Electrochem. Soc. 133 (1986) 1226–1232.
[11] C.B. Shin, D.J. Economou, Effect of transport and reaction on the shape evolution of cavities during wet chemical etching, J. Electrochem. Soc. 136 (1989) 1997–2004.
[12] C.B. Shin, D.J. Economou, Forced and natural convection effects on the shape evolution of cavities during wet chemical etching, J. Electrochem. Soc. 138 (1991) 527–538.
[13] W.J. Li, J.C. Shih, J.D. Mai, C.-M. Ho, J. Liu, Y.-C. Tai, Numerical simulation for the sacrificial release of MEMS square diaphragms, First International Conference on MSMSSA, San Jose, USA, April 1998.
[14] K. Kaneko, T. Noda, M. Sakata, T. Uchiyama, Observation and numerical simulation for wet chemical etching process of semiconductor, in: Proceedings of Fourth ASME-JSME Joint Fluids Engineering Conference, Honolulu, USA, July 6–10 2003.
[15] D. Adalsteinsson, J.A. Sethian, A level set approach to a unified model for etching, deposition and lithography I: algorithms and two-dimensional simulations, J. Comput. Phys. 120 (1995) 128–144.
[16] D. Adalsteinsson, J.A. Sethian, A level set approach to a unified model for etching, deposition and lithography II: three-dimensional simulations, J. Comput. Phys. 122 (1995) 348–366.
[17] A. La Magna, G. D'Arrigo, G. Garozzo, C. Spinella, Computational analysis of etched profile evolution for the derivation of 2D dopant density maps in silicon, Mater. Sci. Eng. B 102 (1–3) (2003) 43–48.
[18] Y.C. Lam, J.C. Chai, P. Rath, H. Zheng, V.M. Murukeshan, A fixed-grid method for chemical etching, Int. Commun. Heat Mass Transfer 31 (8) (2004) 1123–1131.
[19] P. Rath, J.C. Chai, H. Zheng, Y.C. Lam, V.M. Murukeshan, H. Zhu, A fixed-grid approach for diffusion- and reaction-controlled wet chemical etching, Int. J. Heat Mass Transfer 48 (11) (2005) 2140–2149.
[20] P. Rath, J.C. Chai, H. Zheng, Y.C. Lam, V.M. Murukeshan, Modeling two-dimensional diffusion-controlled wet chemical etching using a total concentration approach, Int. J. Heat Mass Transfer 49 (7–8) (2006) 1480–1488.
[21] N. Shamsundar, E.M. Sparrow, Analysis of multidimensional conduction phase change via the enthalpy method, J. Heat Transfer 97 (1975) 333–340.
[22] V. Voller, M. Cross, Accurate solutions of moving boundary problems using the enthalpy method, Int. J. Heat Mass Transfer 24 (1981) 545–556.
[23] C. Prakash, M. Samonds, A.K. Singhal, A fixed-grid numerical methodology for phase change problems involving a moving heat source, Int. J. Heat Mass Transfer 30 (12) (1987) 2690–2694.
[24] A.D. Brent, V.R. Voller, K.J. Reid, Enthalpy–porosity technique for modeling convection–diffusion phase change: application to the melting of a pure metal, Numer. Heat Transfer 13 (1988) 297–318.
[25] X. Zeng, M.D. Xin, An implicit finite difference solution of phase change problems via coupling the enthalpy and moving boundary, HTD-159, Phase Change Heat Transfer ASME (1991) 47–52.
[26] H. Hu, H.A. Argyropoulos, Mathematical modeling of solidification and melting: a review, Model. Simul. Mater. Sci. Eng. 4 (1996) 371–396.
[27] C.K. Chun, S.O. Park, A fixed-grid finite difference method for phase-change problems, Numer. Heat Transfer B 38 (2000) 59–73.
[28] J. Kaenton, G. de Vahl Davis, E. Leonardi, S.S. Leong, A numerical study of anisotropy and convection during solidification, Numer. Heat Transfer B 41 (3-4) (2002) 309–323.
[29] S.V. Patankar, Numerical Heat Transfer and Fluid Flow, first ed., Hemisphere, New York, 1980.